iScience

CellPress
OPEN ACCESS

Article

Ventral hippocampal cholecystokinin interneurons gate contextual reward memory

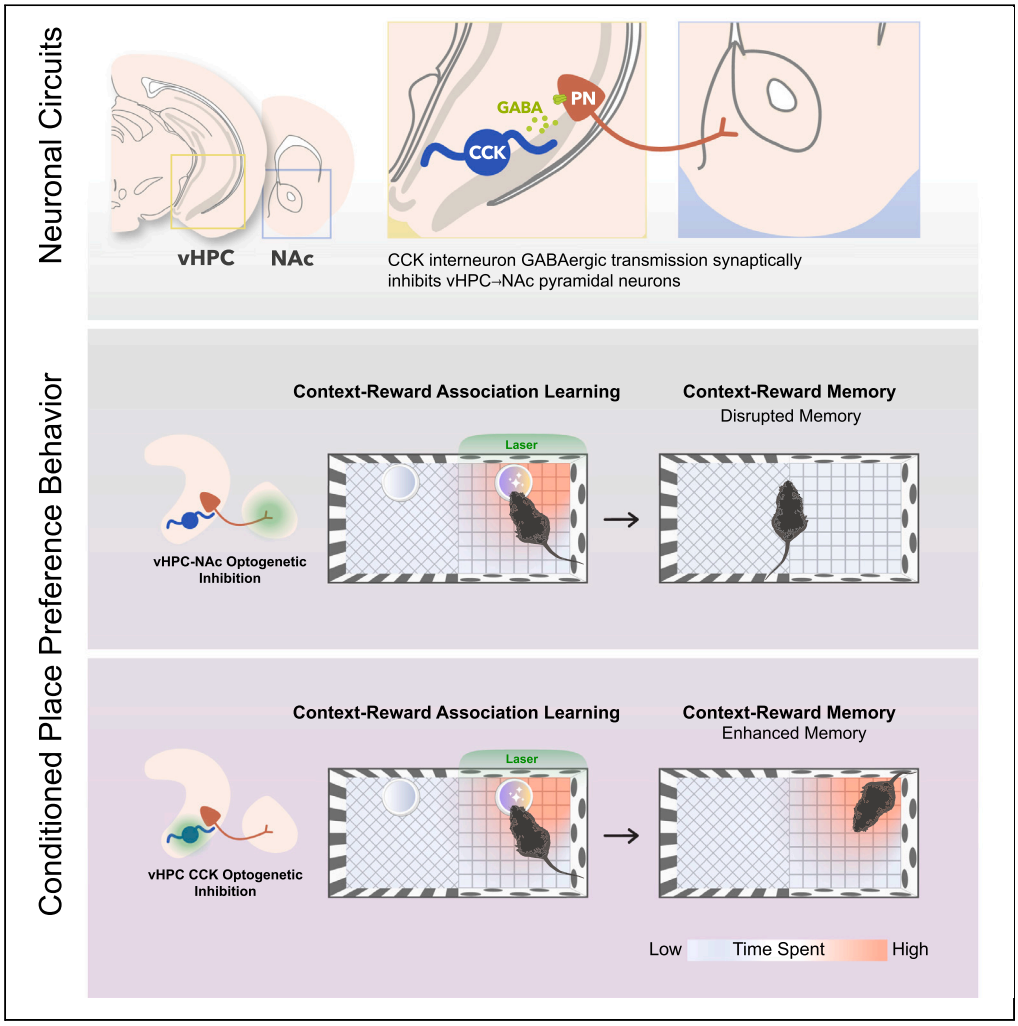

Robin Nguyen, Sanghavy Sivakumaran, Evelyn K. Lambe, Jun Chul Kim

rn2560@columbia.edu (R.N.)
junchul.kim@utoronto.ca (J.C.K.)

Highlights

The vHPC-NAc circuit encodes contexts associated with food reward

vHPC cholecystokinin (CCK) interneurons inhibit vCA1→NAc projecting pyramidal cells

Silencing CCK interneurons in a reward context increased activity of vCA1→NAc cells

Silencing CCK interneurons improved the encoding of contextual reward memory

Nguyen et al., iScience 27, 108824
February 16, 2024
https://doi.org/10.1016/j.isci.2024.108824

iScience

CellPress
OPEN ACCESS

Article

Ventral hippocampal cholecystokinin interneurons gate contextual reward memory

Robin Nguyen,[1,6,*] Sanghavy Sivakumaran,[3] Evelyn K. Lambe,[3,4,5] and Jun Chul Kim[1,2,7,*]

SUMMARY

Associating contexts with rewards depends on hippocampal circuits, with local inhibitory interneurons positioned to play an important role in shaping activity. Here, we demonstrate that the encoding of context-reward memory requires a ventral hippocampus (vHPC) to nucleus accumbens (NAc) circuit that is gated by cholecystokinin (CCK) interneurons. In a sucrose conditioned place preference (CPP) task, optogenetically inhibiting vHPC-NAc terminals impaired the acquisition of place preference. Trans-synaptic rabies tracing revealed vHPC-NAc neurons were monosynaptically innervated by CCK interneurons. Using intersectional genetic targeting of CCK interneurons, *ex vivo* optogenetic activation of CCK interneurons increased GABAergic transmission onto vHPC-NAc neurons, while *in vivo* optogenetic inhibition of CCK interneurons increased cFos in these projection neurons. Notably, CCK interneuron inhibition during sucrose CPP learning increased time spent in the sucrose-associated location, suggesting enhanced place-reward memory. Our findings reveal a previously unknown hippocampal microcircuit crucial for modulating the strength of contextual reward learning.

INTRODUCTION

Animal survival depends on accurately remembering rewarding environments. These contextual memories emerge from the hippocampus,[1,2] yet the neuronal mechanisms underlying their formation remain enigmatic.

GABAergic interneurons and pyramidal neurons are the two primary neuronal classes in the hippocampus.[3] While inhibitory GABAergic interneurons represent a relatively small population,[4] they play an essential role in circuit function and memory.[5] Hippocampal GABAergic interneurons are classified into distinct cell types based on their unique combination of molecular markers, electrophysiological properties, morphology, and connectivity.[6–9] It has been suggested that the varied features among these cell types enable circuit and behavioral specialization.[10–16] Specific classes of GABAergic interneurons may interact with ensembles of hippocampal pyramidal cells to facilitate finely tuned representations underlying memory.[13,17–19] However, the contributions of GABAergic interneuron cell types to different forms of hippocampal memory, such as contextual reward, contextual fear, or social memories remains unclear.

Memory of contexts where emotionally salient events have occurred relies on the ventral hippocampus (vHPC).[20–22] The spatial firing fields of neurons in the vHPC are typically broad,[23,24] effectively mapping entire contexts.[25–27] Additionally, vHPC neurons display selective firing patterns in situations that are associated with emotional valence and that elicit affect-driven behaviors, including behaviors associated with rewards,[25–29] and avoidance and defensive behaviors.[21,25,30–32] Although there have been several studies that show how neuronal activity is related to reward-associated contexts in the vHPC, the specific circuit mechanisms that are responsible for contextual memory of rewards remain poorly understood.

The activation of neurons in the vHPC region varies across different emotional contexts. Specifically, the involvement of pyramidal neurons may be influenced by their projection targets,[27,33] which are highly heterogeneous.[27,34,35] These projection-defined pyramidal neurons in the vHPC may represent distinct functional populations that are recruited based on task demands.[27,30] Notably, outputs of the vHPC to the nucleus accumbens (NAc) have been found to mediate reward-related goal-directed behaviors.[27,35–39] However, the upstream selection factors allowing for their recruitment during behavior have not been clearly elucidated.

CCK interneurons are highly abundant throughout the septotemporal axis of the hippocampus[40] and are likely relevant for spatial memory.[41–44] Furthermore, work from our lab and others have implicated CCK interneurons in dopamine-dependent and reward-related

[1]Department of Psychology, University of Toronto, Toronto, ON, Canada
[2]Department of Cell & Systems Biology, University of Toronto, Toronto, ON, Canada
[3]Department of Physiology, University of Toronto, Toronto, ON, Canada
[4]Department of OBGYN, University of Toronto, Toronto, ON, Canada
[5]Department of Psychiatry, University of Toronto, Toronto, ON, Canada
[6]Present address: Department of Neuroscience, The Kavli Institute for Brain Science, Mortimer B. Zuckerman Mind Brain Behavior Institute, Jerome L. Greene Science Center, Columbia University, New York, NY USA
[7]Lead contact
*Correspondence: rn2560@columbia.edu (R.N.), junchul.kim@utoronto.ca (J.C.K.)
https://doi.org/10.1016/j.isci.2024.108824

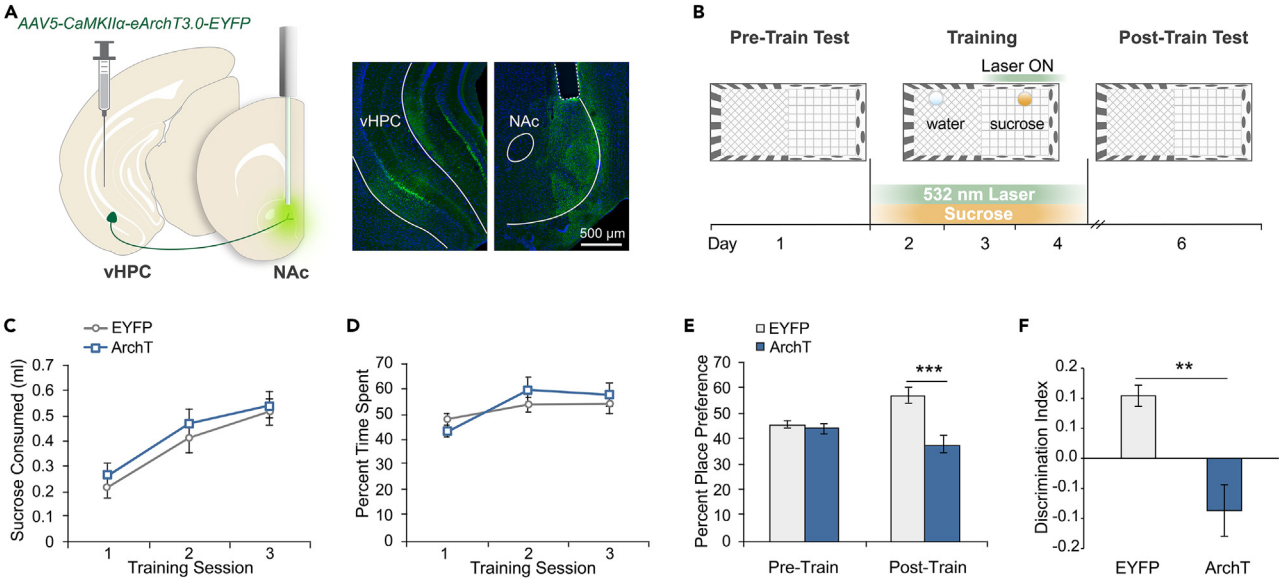

Figure 1. Optogenetic inhibition of vHPC terminals in the NAc during sucrose CPP training impairs memory at test

(A) Left, schematic of vHPC-NAc optogenetic circuit targeting strategy. Right, coronal slices of vHPC and NAc expressing eArchT3.0-EYFP (green).

(B) Behavioral paradigm for closed-loop optogenetic light delivery during sucrose conditioned place preference. Light and sucrose were presented during training sessions only.

(C) Volume of sucrose solution consumed across training sessions. Mixed ANOVA, no main effect of group $F_{(1,\ 15)} = 0.501$, p = 0.486, no group × day interaction, $F_{(2,\ 30)} = 0.24$, p = 0.786.

(D) Percentage of time spent in the light/sucrose-paired context across training sessions. No main effect of group, $F_{(1,\ 15)} = 0.14$, p = 0.714; no group × day interaction, $F_{(2,\ 30)} = 1.77$, p = 0.188.

(E) Percentage of time spent in the reward-context during Pre-train and Post-train preference tests. Mixed ANOVA, group × test interaction, $F_{(1,\ 15)} = 19.41$, p = 0.005. Sidak test for multiple comparisons, Post-train: $t_{(30)} = 5.19$, p < 0.0001; Pre-train: $t_{(30)} = 0.5$, p = 0.855; EYFP: $t_{(15)} = 3.86$, p = 0.003; ArchT: $t_{(15)} = 2.33$, p = 0.068.

(F) Discrimination index of time spent in the reward-context. Unpaired t-test, $t_{(15)} = 3.74$, p = 0.002. EYFP: $N = 8$ mice, ArchT: $N = 9$ mice. Data are presented as mean ± SEM.

behaviors.[10,43,45] Yet the challenge of selectively targeting these cells has left hippocampal CCK interneurons understudied relative to other interneuron cell types, such as parvalbumin or somatostatin interneurons.[5,46]

We hypothesize that the vHPC microcircuit involving CCK interneurons and nucleus accumbens-projecting pyramidal neurons (vHPC-NAc) contributes to the formation of contextual reward memory. We used a combination of dual-recombinase intersectional genetics, rabies-mediated monosynaptic tracing, *ex vivo* electrophysiological recordings, and optogenetic inhibition to target, record, and manipulate the activity of CCK interneurons and vHPC-NAc pyramidal neurons. Our findings demonstrate that local CCK interneurons directly inhibit vHPC-NAc neurons and regulate learning of context-reward associations.

RESULTS

vHPC-NAc circuit is required for contextual reward memory

The vHPC may participate in contextual reward memory by associating specific spatial contexts with rewarding stimuli. This function has been attributed particularly to pyramidal neurons which project to the NAc.[27,38] To test whether the vHPC-NAc circuit is involved in the formation of contextual reward memory, we optogenetically inhibited vHPC terminals in the NAc as mice performed a sucrose conditioned place preference task (CPP). AAV containing archaerhodopsin (ArchT) or a reporter (EYFP) driven by the CaMKIIα promoter (AAV2/5-CaMKIIα-eArchT3.0-EYFP or AAV2/5-CAMKIIα-EYFP) was infused bilaterally into the vHPC and optic fibers were implanted above the NAc shell where the densest vHPC projections were observed (Figure 1A).

These mice were then tested in a modified sucrose CPP paradigm,[38,47] conducted in an apparatus with two compartments (contexts) defined by unique visual and tactile cues. One day prior to the beginning of training, baseline exploration preference was determined in a 5-min test (Pre-train test). Subsequently, on three daily training sessions, sucrose solution (10%) was placed in the context for which mice showed lower baseline preference and water was placed in the opposing context (Figure 1B). Mice freely traversed between the reward- and neutral-contexts for 15 min, and light was delivered through the implanted optic fibers in a closed-loop manner exclusively during occupancy of the reward-context (15 mW of 532 nm continuous laser light measured from the fiber tip).

We did not observe any differences between ArchT and EYFP mice in the amount of sucrose consumed (Figure 1C), or in the percentage of time spent in the reward-context throughout training days (Figure 1D). These results indicate that the vHPC-NAc circuit does not contribute to the intrinsic motivational properties of sucrose reward. Following the final training session 3, we tested preference for the reward-context in the absence of sucrose and light delivery as a measure of memory for the context-reward association (Post-train test). While no group differences were observed during the Pre-train test, during the Post-train test, ArchT mice spent less time in the reward-context compared to EYFP mice (Figures 1E and 1F). Furthermore, whereas EYFP mice spent more time in the reward-context during the Post-relative to the Pre-train test, this was not observed among ArchT mice (Figure 1E). These results suggest that vHPC-NAc terminal inhibition during learning impaired memory encoding of the reward-context, revealing the necessity of activity in the vHPC-NAc circuit for associating rewards with the concurrent spatial context.

vHPC-NAc projecting neurons are innervated by local CCK interneurons

Since we found that inhibiting the activity of vHPC-NAc pyramidal neurons disrupted the formation of contextual reward memory, we hypothesized that endogenous activity suppression by local GABAergic interneurons regulates learning.[48,49] Neural representations in the hippocampus rely on balanced microcircuit interactions between excitatory pyramidal neurons and inhibitory GABAergic interneurons.[13] In particular, we tested the impact of CCK interneurons since they provide strong feedforward inhibition onto pyramidal neurons,[50–53] and have been implicated in dopamine-dependent behaviors,[10] and contextual memory.[41,54]

To investigate whether CCK interneurons monosynaptically innervate vHPC-NAc projecting cells, we used *trans*-synaptic pseudotyped rabies tracing[55] (Figures 2A and 2B). The retrograde virus CAV-2 containing Cre (CAV2-Cre) was infused into the NAc while a cre-dependent AAV vector containing the TVA receptor and optimized glycoprotein (oG) (AAV2/8-hsyn-DIO-TVA-2A-EGFP-2A-oG) were infused into the vHPC. After 2 weeks, G-deleted envelope-A pseudotyped rabies (EnvA-RVdG-mCherry) was infused into the vHPC, and mice were sacrificed 6 days later. In the vHPC, we observed cells positive for both EGFP and mCherry in the ventral CA1 (vCA1) and subiculum (vSub) which constituted the vHPC-NAc 'starter' cell population, and cells singly labeled with mCherry which were the presynaptic input cells (Figure 2A). Immunostaining for GABA and CCK-8 peptide confirmed that a subset of GABA interneurons express CCK (32 $\pm$ 3%), and that CCK is non-selectively expressed in vCA1/vSub cells, with only a small fraction being GABA interneurons (5% $\pm$ 1%). Of the mCherry+ presynaptic cells, 24 $\pm$ 8% were also GABA+ (Figure 2B, middle). Notably, a significant proportion of these presynaptic GABA interneurons in the vCA1/vSub were revealed to be CCK interneurons (45 $\pm$ 10%) (Figure 2B, right).

To determine if CCK interneurons form functional connections with vHPC-NAc projecting cells, we performed *ex vivo* whole cell electrophysiological recordings from NAc projecting pyramidal neurons in the vCA1 while optogenetically stimulating CCK interneurons. To target the excitatory opsin channelrhodopsin (ChR2) to CCK interneurons, CCK-Cre mice were infused with an AAV vector containing Cre-dependent ChR2 driven by the GABA-specific Dlx5/6 promoter (AAV2/1-Dlx5/6-DIO-ChR2-EGFP) into the vHPC (Figure 2C).[56] To visualize vHPC-NAc projecting neurons in the same mice, red retrobeads (590 nm) were infused into the NAc. Blue light (470 nm) delivery to vHPC brain slices directly excited ChR2-EGFP+ CCK interneurons but not EGFP-negative interneurons (Figures 2D–2F). Intrinsic properties of these interneurons did not differ by EGFP status (Table S1), and combined were as follows: input resistance 310 $\pm$ 38 MΩ, resting membrane potential −76 $\pm$ 2 mV, and spike amplitude 73 $\pm$ 2 mV. Stimulation of ChR2-EGFP+ neurons with a short light pulse (1 ms) evoked an action potential under current clamp (Figure 2F, left), and elicited a large inward current under voltage-clamp near resting membrane potential (Figure 2F, middle, right).

Retrobead$^{vHPC\rightarrow NAc}$ neurons were distributed throughout the ventral CA1 and subiculum and were morphologically characteristic of pyramidal neurons (Figure 2D). The intrinsic properties of retrobead$^{vHPC\rightarrow NAc}$ vCA1 pyramidal neurons (Figures 2G–2K) were as follows: input resistance 89 $\pm$ 6 MΩ, resting membrane potential −78 $\pm$ 4 mV, and spike amplitude 82 $\pm$ 3 mV (Table S2). In response to optogenetic stimulation of the local axonal projections of ChR2-EGFP+ CCK interneurons (5 ms pulse), retrobead$^{vHPC\rightarrow NAc}$ neurons exhibited a postsynaptic current which reversed close to the predicted equilibrium potential for a chloride ion current (~75 mV) (Figure 2H). This optogenetically evoked inhibitory response current perturbed the excitability of postsynaptic retrobead$^{vHPC\rightarrow NAc}$ vCA1 pyramidal neurons (Figure 2I). The postsynaptic outward current in these neurons was strongly suppressed by the competitive GABA-A receptor antagonist bicuculline (3 μM, 5 min) (Figures 2I–2K), a suppression that partially reversed after a brief washout period (<10 min) (Figures 2I and 2J). In a minority of neurons (2/7), a bicuculline-resistant outward current was recruited upon repeated stimulation (5 pulses, 10 Hz), which was sensitive to suppression by the GABA-B receptor antagonist CGP 35348 (1 μM) (Figure 2K). Taken together, these findings suggest CCK interneurons provide functional GABAergic innervation of vHPC pyramidal neurons that project to the NAc.

Intersectional genetic targeting of vHPC CCK interneurons

To evaluate the contribution of CCK interneurons to behavior, we expressed ArchT selectively in CCK interneurons to silence their activity *in vivo*. Due to nonspecific CCK neuropeptide expression in both GABA interneurons and pyramidal neurons,[57] CCK interneurons cannot be selectively targeted with conventional single recombinase methods. Therefore, we applied a dual recombinase intersectional approach,[58] using both the Cre/lox and Flpe/FRT systems, to genetically access CCK interneurons.[40] ArchT expression was targeted to CCK interneurons by crossing the CCK-Cre line with Dlx5/6-Flpe, and their double transgenic offspring with the Cre and Flpe-dependent RC::PFArchT-EGFP line. In the resulting CCK-Dlx5/6-FrePe triple transgenic mice (referred to as CCK-ArchT mice from here on), Flpe- and Cre-mediated excisions of the two transcriptional stop cassettes, the first flanked by *loxP* sites and the second by FRT sites, resulted in ArchT-EGFP expression selectively in CCK interneurons (Figures 3A and 3B). Consistent with previous findings on the distribution of CCK interneurons in the

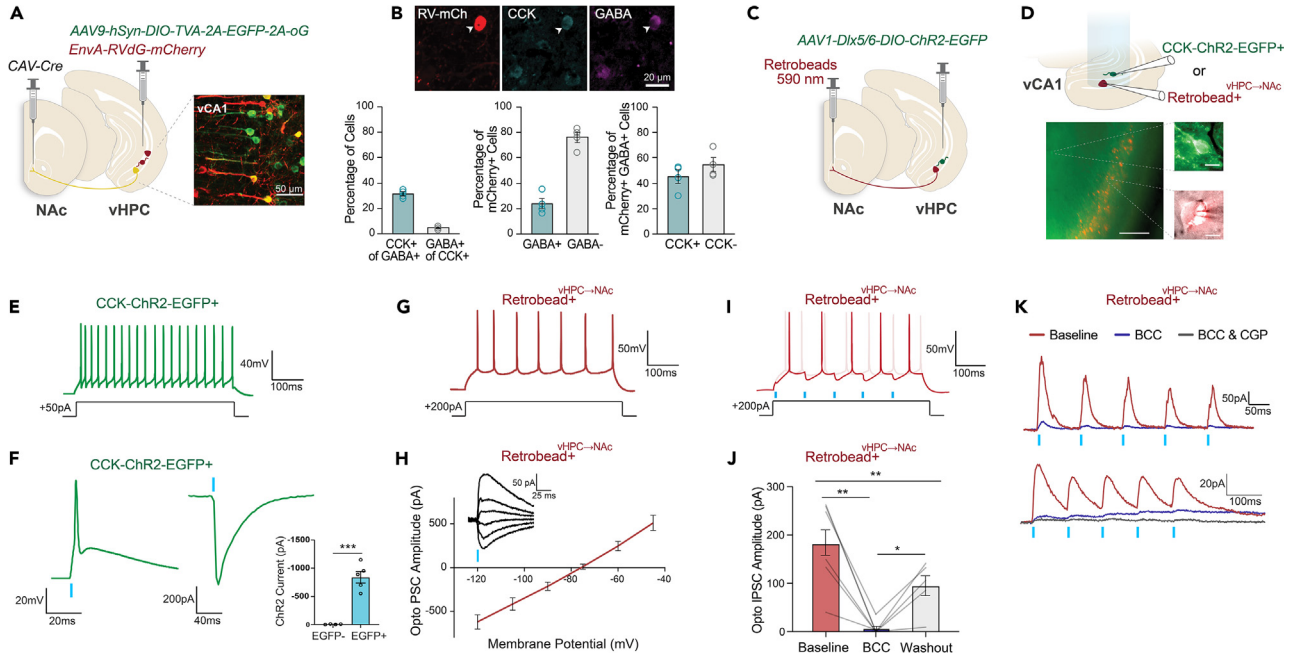

Figure 2. CCK interneurons in vHPC provide monosynaptic GABAergic inhibition of CA1 pyramidal neurons that project to nucleus accumbens (NAc)

(A) Schematic of targeting approach for *trans*-synaptic pseudotyped rabies tracing from vHPC-NAc projecting neurons. Inset, representative image of starter cells double-labelled with EGFP and mCherry, and presynaptic input cells singly labeled with mCherry in the vCA1.

(B) Top, representative immunostaining for CCK-8 (cy5,blue) and GABA (405 nm, magenta) against mCherry expression. Bottom left, percentage of vCA1 cells immunoreactive for CCK-8 and GABA. Bottom middle, percentage of mCherry+ presynaptic input cells immunoreactive for GABA. Bottom right, percentage of GABAergic presynaptic input cells (double-labelled with mCherry and GABA) that are immunoreactive for CCK-8. $N = 4$ mice.

(C) Schematic of experimental strategy to express ChR2 in vHPC CCK interneurons and simultaneous retrograde tracing of vHPC-NAc projecting neurons with retrobeads.

(D) Top, schematic of *ex vivo* electrophysiology in vCA1 with blue light illumination to stimulate ChR2-EGFP+ CCK interneurons at the level of either their cell bodies or their axons in the vCA1 pyramidal cell layer. Recordings were made from either ChR2-EGFP+ CCK interneurons or retrobead+$^{vHPC \rightarrow NAc}$ pyramidal neurons. Bottom, representative merged fluorescence and brightfield images of vCA1 (scale bar, 100 µm). Top right, ChR2-EGFP+ CCK interneuron (green, scale bar, 5 µm). Bottom right, merged fluorescence and IR-DIC images of a recording pipette patching a retrobead$^{vHPC \rightarrow NAc}$ pyramidal neuron (red, scale bar, 5 µm).

(E) Electrophysiological response of a ChR2-EGFP+ CCK interneuron to a step of depolarizing current.

(F) Brief optogenetic stimulation (1 ms pulse, vertical blue line) excites a ChR2-EGFP+ CCK interneuron, in current-clamp from rest (left), and in voltage-clamp at −75 mV (middle, right). Recordings in interneurons by EGFP status shows selective excitation as measured by inward currents in voltage-clamp (unpaired *t* test: $t_{(7)} = 7.2$, $p = 0.0002$; $N = 4$ mice).

(G) Electrophysiological response of a retrobead$^{vHPC \rightarrow NAc}$ vCA1 pyramidal neuron to a step pulse of depolarizing current.

(H) The optogenetically evoked postsynaptic response reverses near the predicted equilibrium potential for a chloride ion current; $N = 4$ mice. Inset, example voltage-clamp traces across a range of pyramidal cell holding potentials.

(I) Optogenetically evoked responses perturb the excitability of a postsynaptic retrobead$^{vHPC \rightarrow NAc}$ vCA1 pyramidal neuron. Lighter trace shows excitability without optogenetic stimulation.

(J) Pharmacological characterization confirms that optogenetically-elicited outward currents (Vh = −60 mV) are suppressed by the competitive antagonist of GABA-A receptors (bicuculline: BCC, 3 µM). One-way repeated measures ANOVA, main effect of treatment, $F_{(1.445,\ 6.502)} = 15.83$; $p = 0.004$. Tukey's tests: baseline vs. bicuculline: $p = 0.01$; bicuculline vs. washout: $p = 0.02$; $N = 4$ mice.

(K) Examples from two retrobead-positive vCA1 pyramidal neurons illustrating currents elicited by brief trains of optogenetic stimulation at baseline and upon blockade of GABA receptors. Data are presented as mean ± SEM.

hippocampus,[59–61] the labeled ArchT-EGFP+ neurons were observed across all layers of the ventral CA1 but were most abundant in the stratum pyramidale (Figure 3C). A large majority of these neurons were immunoreactive for CCK-8 and GABA, while only a small percentage were immunoreactive for PV, SOM, or VIP (Figure 3D), indicating high selectivity of the targeting approach for CCK interneurons.

vHPC CCK interneurons regulate activity of vHPC-NAc projecting neurons *in vivo*

We observed that wildtype C57BL6/J mice that had been exposed to a context containing sucrose reward displayed increased cFos expression in the vHPC relative to mice exposed to sucrose in their home-cage, to a neutral context containing water, or to mice that had simply remained in the home-cage (Figures 4A and 4B). This finding indicates that vHPC neurons are strongly recruited by rewarding contexts, which

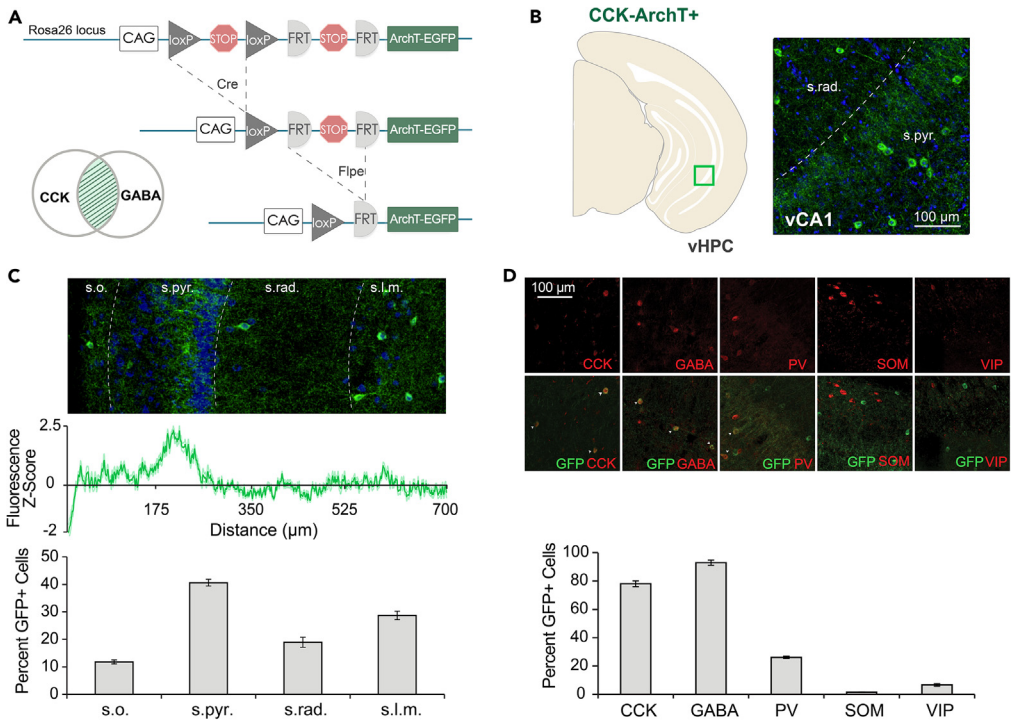

Figure 3. Intersectional genetic expression of ArchT in vHPC CCK interneurons

(A) Dual recombinase-responsive reporter allele, RC::PFArchT-EGFP, contains two transcriptional stop cassettes flanked by *loxP* and FRT sites. Cre- and Flpe-mediated excisions result in ArchT-EGFP expression in CCK interneurons.

(B) Right, representative ArchT-EGFP expression (green) in vCA1 (boxed area in schematic) of a CCK-ArchT mouse.

(C) Top, representative ArchT-EGFP expression across vCA1 strata. Middle, normalized fluorescence intensity (*Z* score) of ArchT-EGFP expression as a function of distance from the alveus. Bottom, percentage of ArchT-EGFP positive cells in each stratum of vCA1. One-way repeated measures ANOVA, $F_{(1.31,\ 5.25)} = 17.54$, $p = 0.0063$, $N = 5$ mice. s.o. stratum oriens, s.pyr. stratum pyramidale, s.rad. stratum radiatum, s.l.m. stratum lacunosum-moleculare.

(D) Top, representative immunostaining for GABA interneuron markers (red) against EGFP expression in CCK-ArchT mice. Bottom, percentage of ArchT-EGFP positive cells immunoreactive for given GABA interneuron marker. One-way ANOVA, $F_{(4,\ 10)} = 932.6$, $p < 0.0001$, $N = 3$ mice. Data are presented as mean ± SEM.

led us to ask whether local CCK interneurons may regulate the neuronal recruitment, including of vHPC-NAc projecting pyramidal neurons. We therefore employed the above intersectional optogenetic strategy to evaluate the effect of inhibiting vHPC CCK interneurons on the activity of vHPC-NAc projecting pyramidal neurons as mice explored a context containing sucrose reward.

In CCK-ArchT mice, the retrograde tracer cholera toxin subunit B (CTB) conjugated to Alexa Fluor 555 was infused into the NAc shell resulting in CTB labeling of cell bodies in the ventral CA1 and subiculum (Figures 4C and 4G). These mice were also implanted with bilateral optic fibers positioned above the vHPC (vCA1/subiculum regions). First, mice were exposed to a context containing sucrose solution for 10 min during which light was delivered to inhibit vHPC CCK interneurons (Figure 4D). Since we hypothesized that silencing CCK interneurons would disinhibit vHPC-NAc projecting neurons recruited by reward, a low concentration of sucrose solution (1%) was provided.[62] After context-reward exposure, mice were placed in their home cage for 60 min to allow cFos protein expression to accumulate and were then sacrificed.[63] Inhibiting CCK interneurons in a reward-containing context significantly increased the density of cFos-positive neurons in the vHPC (Figure 4F). Quantification of neurons that were double-labeled for $CTB^{vHPC \rightarrow NAc}$ and cFos revealed an increase in the percentage of $CTB^{vHPC \rightarrow NAc}$ neurons expressing cFos in CCK-ArchT + compared to CCK-ArchT-mice (Figure 4H). Therefore, inhibiting CCK interneurons in a context containing sucrose reward increased cFos expression in vHPC neurons that project to the NAc.

CCK interneuron inhibition enhances contextual reward memory

Since CCK interneurons were found to influence the activity of vHPC-NAc projecting neurons, we asked whether CCK interneurons may also be involved in the acquisition of contextual reward memory. We performed the sucrose CPP task as described in the previous section using 1% sucrose solution. Light was delivered to the vHPC of CCK-ArchT mice throughout the three training days exclusively during occupancy of the sucrose-containing context (Figures 5A–5C). During training, we did not observe any differences between CCK-ArchT+ and CCK-ArchT-mice in the amount of sucrose consumed (Figure 5B), or in the percentage of time spent in the reward-context (Figure 5C). In the place preference test, both groups spent a higher percentage of time in the reward-context during the Post-train test relative to the Pre-train test (Figure 5D). However, CCK-ArchT + mice exhibited significantly greater preference for the reward-context compared to CCK-ArchT-mice (Figures 5D and

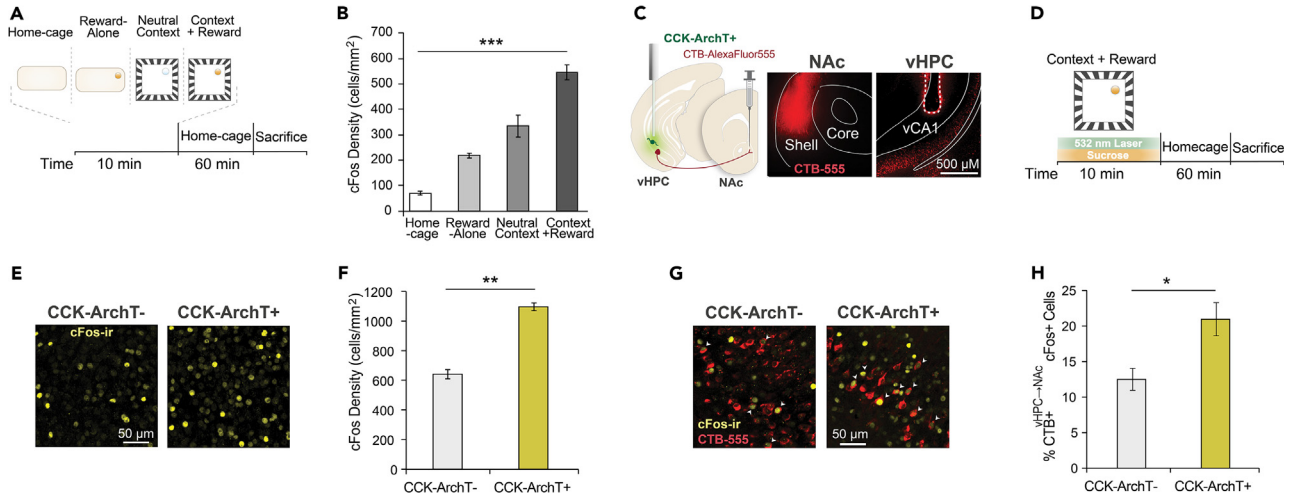

Figure 4. vHPC cFos expression following CCK interneuron inhibition during exposure to a context containing reward

(A) Time course for cFos labeling experiment following exposure to sucrose solution in the home-cage, to a neutral water-containing context, to the context with sucrose reward present, or remaining in the home-cage.

(B) Density of cFos-immunoreactive cells in the vHPC. One-way ANOVA, $F_{(3,16)} = 54.68$, $p < 0.0001$; Tukey's multiple comparisons test, Home-cage vs. Reward-Alone: $p = 0.0065$, Home-cage vs. Neutral Context: $p < 0.0001$, Home-cage vs. Context+Reward: $p < 0.0001$, Reward-Alone vs. Neutral Context: $p = 0.038$, Reward-Alone vs. Context+Reward: $p < 0.0001$, Neutral Context vs. Context+Reward: $p = 0.0002$. $N = 5$ mice in each condition.

(C) Left, schematic of CTB-mediated retrograde tracing from nucleus accumbens combined with optogenetic inhibition of CCK interneurons in vHPC. Right, representative image of CTB-Alexa-Fluor-555 infusion in NAc shell, and of CTB $^{vHPC \rightarrow NAc}$ retrogradely labeled cell bodies and optic fiber in vHPC.

(D) Time course for optogenetic cFos experiment. Light was delivered during exposure to a context containing sucrose.

(E) Representative images of cFos-immunoreactivity in the vHPC from CCK-ArchT- (left) and CCK-ArchT+ (right) mice.

(F) Density of cFos-immunoreactive cells in the vHPC. Unpaired t-test, $t_{(9)} = 4.28$, $p = 0.002$; CCK-ArchT-: $N = 6$, CCK-ArchT+: $N = 5$.

(G) Representative overlap between cFos-immunoreactivity and CTB$^{vHPC \rightarrow NAc}$ labeling in the vHPC of CCK-ArchT- (left) and CCK-ArchT+ (right) mice.

(H) Percentage of CTB$^{vHPC \rightarrow NAc}$ cells in the vHPC immunoreactive for cFos. Unpaired t-test, $t_{(8)} = 3.03$, $p = 0.016$; CCK-ArchT-: $N = 5$, CCK-ArchT+: $N = 5$. Data are presented as mean ± SEM.

5E). To determine the specificity of this enhanced place preference memory, we subdivided the reward-context into quadrants and measured the time spent in each zone (Figures 5F and 5G). Notably, CCK-ArchT + mice spent a significantly greater percentage of time in the zone where the sucrose dish was previously located compared to CCK-ArchT-mice (Figures 5G and 5H). These findings indicate that CCK interneuron inhibition strengthened learning of the context-reward association, resulting in enhanced memory of the location where reward was previously encountered.

Alternatively, silencing CCK interneurons may have influenced preference behavior during the Post-train test session by altering the reinforcing properties of the context itself,[36] although, no direct effects of light delivery on preference were observed during sucrose CPP training. Another possibility is that mice may be detecting a mismatch in light-delivery during training and test that drives context exploration. We addressed these possibilities by inhibiting CCK interneurons in the same manner as the previous experiment but in the absence of sucrose during training. No significant differences were observed between CCK-ArchT+ and CCK-ArchT-mice in the percentage of time spent in the light-paired context during training (Figures 6A and 6B), or during the Pre- and Post-train preference tests (Figure 6C). Thus, CCK interneurons do not contribute to intrinsic preference behaviors in neutral contexts, and rather, influences memory-guided preference of contexts associated with reward.

CCK interneuron inhibition does not alter contextual fear or social memory

To test whether CCK interneuron inhibition of vHPC-NAc projecting neurons is specific for context-reward memory, we additionally investigated two other forms of memory. The vHPC has also been implicated in fear memory and social memory.[21,30,37,64] We evaluated whether vHPC CCK interneurons may be involved in the formation of contextual fear memory by optogenetically inhibiting CCK interneurons during contextual fear conditioning. No significant differences in freezing levels were found between CCK-ArchT+ and CCK-ArchT-mice during the test sessions in the fear conditioned context (Context A) or in a novel context (Context B) (Figure 6D), indicating CCK interneuron inhibition did not affect contextual fear memory learning or specificity. Furthermore, we tested the role of CCK interneurons in the acquisition of social memory in a three-chamber social recognition memory task.[65] Light was delivered during the encoding phase only when mice occupied the chamber containing a social conspecific stimulus. CCK interneuron inhibition did not affect social interaction during the encoding phase (Figure 6E), or during the social recognition memory test (Figure 6F). Together, these experiments demonstrate that CCK interneuron mediated inhibition of vHPC-NAc projecting neurons selectively controls context-reward memory.

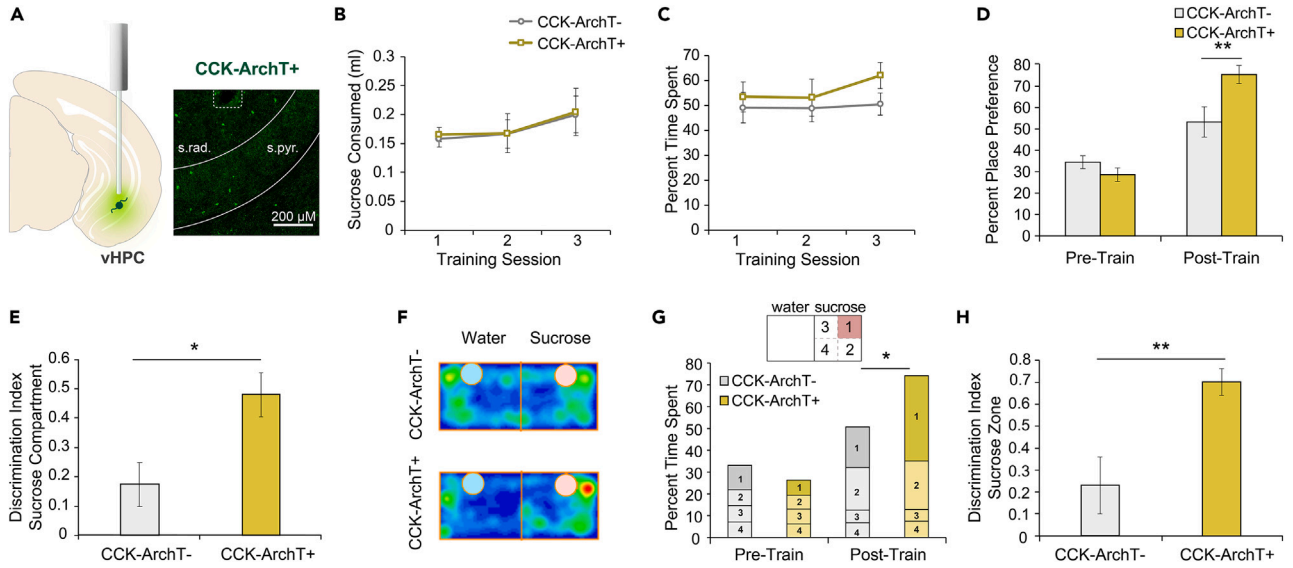

Figure 5. vHPC CCK interneuron inhibition during sucrose conditioned place preference training enhances memory at test

(A) Left, schematic of optogenetic targeting strategy of vHPC CCK interneurons. Right, magnified coronal image of vCA1 CCK interneurons expressing ArchT-EGFP.

(B) Volume of sucrose solution consumed across training sessions. Mixed ANOVA, no main effect of group $F_{(1, 15)} = 0.03$, $p = 0.875$, no group × day interaction, $F_{(2, 30)} = 0.01$, $p = 0.991$.

(C) Percentage of time spent in the light/sucrose-paired context across training sessions. No main effect of group, $F_{(1, 15)} = 0.84$, $p = 0.374$; no group × day interaction, $F_{(2, 30)} = 0.68$, $p = 0.517$.

(D) Percentage of time spent in the reward-context during the Pre-train and Post-train preference tests. Mixed ANOVA, main effect of test, $F_{(1, 15)} = 46.05$, $p < 0.0001$; group × test interaction, $F_{(1, 15)} = 10.34$, $p = 0.006$. Sidak test, Post-train: $t_{(30)} = 3.59$, $p = 0.002$, Pre-train: $t_{(30)} = 0.91$, $p = 0.6$.

(E) Discrimination index of time spent in the reward-context. Unpaired t-test, $t_{(15)} = 2.88$, $p = 0.011$.

(F) Group averaged heat maps of occupation time in the CPP apparatus during the Post-train test.

(G) Percentage of time spent in individual zones of the reward-context during the Pre- and Post-train tests. Mixed ANOVA, group × context × zone interaction, $F_{(3, 48)} = 2.90$, $p = 0.044$. Post-train: Sidak test, $t_{(14.95)} = 2.97$, $p = 0.038$.

(H) Discrimination index of time spent in the reward zone. Unpaired t-test, $t_{(15)} = 3.45$, $p = 0.004$. CCK-ArchT-, $N = 8$; CCK-ArchT+, $N = 9$. Data are presented as mean ± SEM.

DISCUSSION

To successfully predict the availability of future rewards, animals must rapidly form and store internal representations of rewarding environments. Yet, adaptive behavior requires learning to be proportional to the probability and motivational value of rewards,[66] with maladaptive learning associated with conditions such as addiction and depression.[67,68]

Our study demonstrates that context-reward memory encoding is governed by a ventral hippocampal circuit in which CCK interneurons regulate CA1 pyramidal neurons projecting to the NAc. This work demonstrates that the strength of learning can be controlled by the balance of excitation in this circuit. Specifically, we found that, within the vHPC, inhibitory CCK interneurons monosynaptically innervate and modulate the excitability of pyramidal neurons projecting to the NAc. In reward-containing environments, inhibiting CCK interneuron activity increased the number of activated vHPC-NAc neurons and enhanced contextual reward learning. Meanwhile, inhibiting activity in the vHPC-NAc pathway had the opposite effect of impairing learning.

Context-reward circuit in perspective

Pyramidal neurons in the vCA1 are heterogeneous in that they express unique genetic markers,[69,70] and send outputs to a diverse array of downstream targets.[34] Projection-defined pyramidal neurons may represent functional populations and have been reported to exhibit task-selective recruitment.[27,30,35,39] In the present study, we found that inhibiting vHPC terminals in the NAc as mice were in a context containing sucrose reward, decreased subsequent preference for that context. Previous findings suggest that this outcome is unlikely to be due to alterations in innate preference or aversion to the light-paired context.[36] Instead, vHPC projections to the NAc may be essential for associating a natural food reward with spatial contextual information. This finding aligns with previous studies demonstrating the involvement of this pathway in conditioned place preference for social reward,[38] and drug reward.[39] During reward learning, environmental cues gain incentive salience and come to elicit goal-directed behaviors.[71] The ability of spatial cues to drive reward seeking relies on coordinated activity between the hippocampus and NAc.[72–74] Both the dorsal and vHPC exhibit reward context-specific firing patterns following conditioning with rewards,[26,27,75–77] which in turn likely drives the context selectivity of NAc medium spiny neurons.[76,78,79]

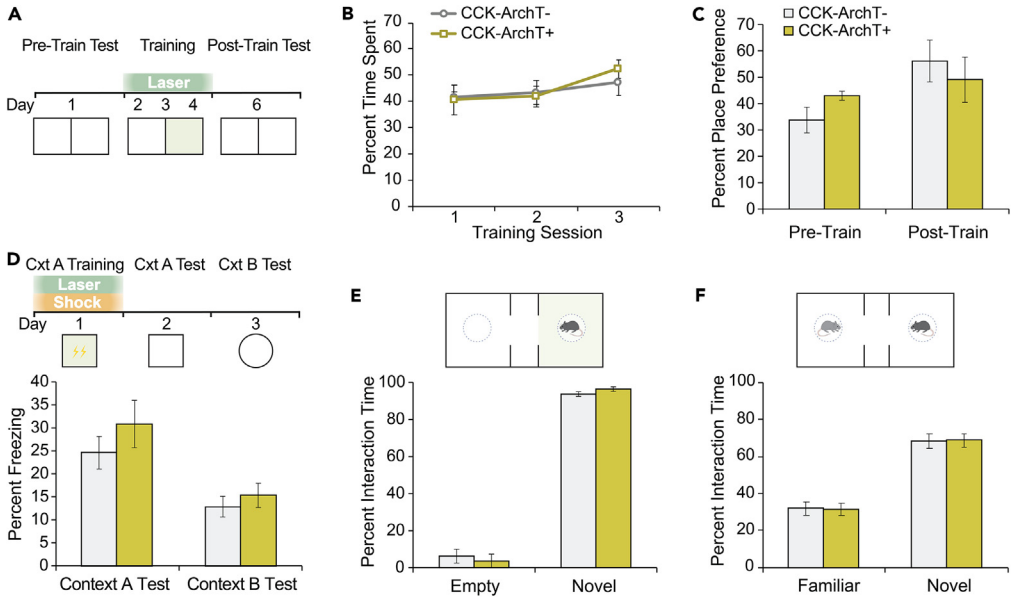

Figure 6. vHPC CCK interneuron silencing does not affect encoding of alternate forms of memory

(A) Behavioral paradigm for repeated real-time place preference with closed-loop optogenetic inhibition during training.

(B) Percentage of time spent in the light-paired side across training sessions. Mixed ANOVA, no main effect of group, $F_{(1,11)} = 0.04$, p = 0.842; no group × training day interaction, $F_{(2,22)} = 0.49$, p = 0.62; CCK-ArchT-: *N* = 8 mice, CCK-ArchT+: *N* = 5 mice.

(C) Percentage of time spent in the light paired side during the pre-training and post-training preference tests. Mixed ANOVA, no main effect of group, $F_{(1,22)} = 3.07$, p = 0.094; no group × test day interaction, $F_{(1,22)} = 0.77$, p = 0.391.

(D) Behavioral paradigm for contextual fear conditioning with optogenetic inhibition during fear training (*Top*). Percentage of freezing in contexts A and B at test. Unpaired t-test, Context A: $t_{(15)} = 0.97$, p = 0.346; Context B: t-test, $t_{(15)} = 0.70$, p = 0.496. CCK-ArchT-: *N* = 8 mice, CCK-ArchT+: *N* = 9 mice.

(E) Schematic of the encoding phase of social recognition memory with closed-loop optogenetic inhibition in the compartment containing the novel conspecific (*Top*). Percentage of time spent interacting with the empty cage or novel conspecific (*Bottom*). Mixed ANOVA, no main effect of group, $F_{(1,16)} = 0$, p > *0.999*; no group × stimulus interaction, $F_{(1,16)} = 0.802$, p = 0.384; CCK-ArchT-: *N* = 6 mice, CCK-ArchT+: *N* = 4 mice.

(F) Schematic of the social recognition memory test phase (*Top*). Percentage of time spent interacting with the familiar or novel conspecific (*Bottom*). Mixed ANOVA, no main effect of group, $F_{(1,16)} = 0$, p > *0.999*; no group × stimulus interaction, $F_{(1,16)} = 0.019$, p = 0.893. Data are presented as mean ± SEM.

Importantly, our finding of enhanced memory for contexts associated with reward resulted from inhibiting vHPC CCK interneurons exclusively in the reward-paired context. A potential mechanism explaining this finding relates to the context specificity of vHPC pyramidal neurons. CCK interneuron inhibition may have promoted the reward-context specific activity of NAc-projecting pyramidal neurons in the vHPC, leading to improved context encoding and discrimination. Future studies could evaluate this hypothesis by simultaneously inhibiting CCK interneurons and recording the activity of vHPC-NAc neurons in a contextual reward learning task. Another potential approach would be to assess the impact of optogenetically stimulating CCK interneurons on vHPC-NAc neuronal activity during context-reward learning and its subsequent effects on memory formation. We postulate that stimulating CCK interneurons in the rewarding context could diminish the activity of vHPC-NAc neurons selectively in that context leading to impaired context-reward memory. However, the spatially unrestricted inhibition associated with optogenetic stimulation of GABA interneurons,[80] coupled with variable behavioral outcomes dependent on stimulation parameters and opsin variants,[81–84] could complicate the interpretation of results.

Clinical relevance of mechanism, caveats, and future directions

We optogenetically inhibited vHPC CCK interneurons during memory tests that were previously shown to be dependent on the vHPC.[30,37–39,64] Inhibiting CCK interneurons enhanced the formation of contextual reward memory. In contrast, the same manipulation did not affect the formation of contextual fear memory or social memory, indicating CCK interneurons do not strongly regulate the circuits mediating these behaviors. Specifically, the vHPC sends prominent projections to the basolateral amygdala to support contextual fear memory,[21,30] and to the medial prefrontal cortex for social memory.[64] Outputs of the vHPC to the NAc have also been reported to contribute to the retrieval of social memory,[37] but this was observed in a social recognition memory task that differed from the one used in the current study.[64] The selective involvement of CCK interneurons in contextual reward memory may indicate a biased functional connectivity with vHPC-NAc pyramidal neurons.[12,85] This possibility would need to be examined by comparing the inhibitory impact of CCK interneurons on multiple circuit-defined pyramidal neurons *in vivo*. Alternatively, vHPC CCK interneurons may play a more essential role in memories that are acquired gradually across repeated experiences as opposed to rapidly formed associative or incidental memories.

How would the unique properties of CCK interneurons allow for this population to act as a flexible gate in selecting pyramidal cell ensembles underlying context-reward memory? As we observed in the current study, CCK interneurons are distributed across layers in the CA1 and according to their axon localization are primarily dendrite-targeting or basket cells.[59–61,86] While CCK interneurons express several neuromodulatory receptors that would maintain their activity during wakefulness,[87,88] most intriguingly, they possess a unique 'off' switch, expressing high amounts of the CB1 receptor relative to other GABA interneuron subtypes and pyramidal neurons.[87,89,90] Stimulation of this receptor by endocannabinoids permits suppression of inhibition and long-term depression.[41,91–94] This mechanism would aid the encoding of context-reward associations in the hippocampus by amplifying the gain of spatial representations coinciding with reward.[95] Accordingly, we observed that inhibiting CCK interneurons both increased the number of activated NAc-projecting cells and improved contextual reward memory, consistent with an active role for this inhibitory circuit in regulating recruitment of pyramidal neurons to memory ensembles. Our preclinical work underscores the likely importance of CCK interneurons in optimizing context-reward memories, raising questions about the neuropathological consequences of damage or disrupted signaling to these neurons.[96–99]

Conclusions

In summary, we identified a local inhibitory microcircuit in the vHPC in which CCK interneurons modulate the excitability of nucleus accumbens projecting pyramidal neurons to specifically control the strength of contextual reward learning. Thus, CCK interneurons may play a critical role for ensuring that contextual reward learning accumulates with experience over time, allowing for flexible reward-seeking behavior in dynamic and unpredictable environments.

Limitations of the study

For the optogenetic behavioral experiments, ArchT was broadly expressed in forebrain CCK interneurons. CCK interneuron silencing was then restricted to the ventral CA1/subiculum by placing the optic fiber above this region and carefully controlling laser light power. However, it cannot be ruled out that CCK interneurons in adjacent areas were affected. Furthermore, this study found that a significant proportion (26%) of CCK-ArchT cells were immunopositive for PV. Since we did not perform experiments to inhibit PV interneurons, it is unknown whether the effects of inhibiting CCK interneurons may be partially accounted for by the disruption of PV interneurons.

STAR★METHODS

Detailed methods are provided in the online version of this paper and include the following:

- KEY RESOURCES TABLE
- RESOURCE AVAILABILITY
  - Lead contact
  - Materials availability
  - Data and code availability
- EXPERIMENTAL MODEL AND STUDY PARTICIPANT DETAILS
- METHOD DETAILS
  - Stereotaxic surgery
  - Behavioural Apparatuses and testing procedures
  - cFos behavioural procedures
  - *Ex vivo* electrophysiology
  - Histology
- QUANTIFICATION AND STATISTICAL ANALYSIS

SUPPLEMENTAL INFORMATION

Supplemental information can be found online at https://doi.org/10.1016/j.isci.2024.108824.

ACKNOWLEDGMENTS

We thank members of the Kim laboratory for discussions of the project. This work was supported by the following grants: Natural Sciences and Engineering Research Council of Canada (NSERC) Discovery MOP 506730 (J.C.K.), Canadian Institutes of Health Research (CIHR) MOP 507489 (J.C.K.), NSERC Discovery Grant (E.K.L.), and CIHR PJT-178372 (E.K.L.).

AUTHOR CONTRIBUTIONS

Conceptualization: R.N. and J.C.K.
Methodology: R.N. and S.S.
Investigation: R.N. and S.S.
Visualization: R.N., S.S., and E.K.L.
Funding acquisition: J.C.K. and E.K.L.

Supervision: J.C.K. and E.K.L.
Writing – original draft: R.N. and S.S.
Writing – review and editing: R.N., J.C.K., and E.K.L.

DECLARATION OF INTERESTS

The authors declare no competing interests.

Received: April 21, 2023
Revised: November 6, 2023
Accepted: January 3, 2024
Published: January 9, 2024

REFERENCES

1. Ross, T.W., and Easton, A. (2022). The Hippocampal Horizon: Constructing and Segmenting Experience for Episodic Memory. Neurosci. Biobehav. Rev. *132*, 181–196.
2. Fanselow, M.S., and Dong, H.W. (2010). Are the dorsal and ventral hippocampus functionally distinct structures? Neuron *65*, 7–19.
3. Pelkey, K.A., Chittajallu, R., Craig, M.T., Tricoire, L., Wester, J.C., and McBain, C.J. (2017). Hippocampal GABAergic inhibitory interneurons. Physiol. Rev. *97*, 1619–1747.
4. Bezaire, M.J., and Soltesz, I. (2013). Quantitative assessment of CA1 local circuits: Knowledge base for interneuron-pyramidal cell connectivity. Hippocampus *23*, 751–785.
5. Tzilivaki, A., Tukker, J.J., Maier, N., Poirazi, P., Sammons, R.P., and Schmitz, D. (2023). Hippocampal GABAergic interneurons and memory. Neuron *111*, 3154–3175.
6. Kepecs, A., and Fishell, G. (2014). Interneuron cell types are fit to function. Nature *505*, 318–326.
7. Harris, K.D., Hochgerner, H., Skene, N.G., Magno, L., Katona, L., Bengtsson Gonzales, C., Somogyi, P., Kessaris, N., Linnarsson, S., and Hjerling-Leffler, J. (2018). Classes and continua of hippocampal CA1 inhibitory neurons revealed by single-cell transcriptomics. PLoS Biol. *16*, e2006387.
8. Gouwens, N.W., Sorensen, S.A., Baftizadeh, F., Budzillo, A., Lee, B.R., Jarsky, T., Alfiler, L., Baker, K., Barkan, E., Berry, K., et al. (2020). Integrated Morphoelectric and Transcriptomic Classification of Cortical GABAergic Cells. Cell *183*, 935–953.e19.
9. Klausberger, T., and Somogyi, P. (2008). Neuronal diversity and temporal dynamics: the unity of hippocampal circuit operations. Science (New York, N.Y.) *321*, 53–57.
10. Nguyen, R., Morrissey, M.D., Mahadevan, V., Cajanding, J.D., Woodin, M.A., Yeomans, J.S., Takehara-Nishiuchi, K., and Kim, J.C. (2014). Parvalbumin and GAD65 interneuron inhibition in the ventral hippocampus induces distinct behavioral deficits relevant to schizophrenia. J. Neurosci. *34*, 14948–14960.
11. Nguyen, R., Venkatesan, S., Binko, M., Bang, J.Y., Cajanding, J.D., Briggs, C., Sargin, D., Imayoshi, I., Lambe, E.K., and Kim, J.C. (2020). Cholecystokinin-Expressing Interneurons of the Medial Prefrontal Cortex Mediate Working Memory Retrieval. J. Neurosci. *40*, 2314–2331.
12. Lee, S.H., Marchionni, I., Bezaire, M., Varga, C., Danielson, N., Lovett-Barron, M., Losonczy, A., and Soltesz, I. (2014). Parvalbumin-positive basket cells differentiate among hippocampal pyramidal cells. Neuron *82*, 1129–1144.
13. Royer, S., Zemelman, B.V., Losonczy, A., Kim, J., Chance, F., Magee, J.C., and Buzsáki, G. (2012). Control of timing, rate and bursts of hippocampal place cells by dendritic and somatic inhibition. Nat. Neurosci. *15*, 769–775.
14. Kim, D., Jeong, H., Lee, J., Ghim, J.W., Her, E.S., Lee, S.H., and Jung, M.W. (2016). Distinct Roles of Parvalbumin- and Somatostatin-Expressing Interneurons in Working Memory. Neuron *92*, 902–915.
15. Abbas, A.I., Sundiang, M.J.M., Henoch, B., Morton, M.P., Bolkan, S.S., Park, A.J., Harris, A.Z., Kellendonk, C., and Gordon, J.A. (2018). Somatostatin Interneurons Facilitate Hippocampal-Prefrontal Synchrony and Prefrontal Spatial Encoding. Neuron *100*, 926–939.e3.
16. Soltesz, I., and Losonczy, A. (2018). CA1 pyramidal cell diversity enabling parallel information processing in the hippocampus. Nat. Neurosci. *21*, 484–493.
17. Lovett-Barron, M., Kaifosh, P., Kheirbek, M.A., Danielson, N., Zaremba, J.D., Reardon, T.R., Turi, G.F., Hen, R., Zemelman, B.V., and Losonczy, A. (2014). Dendritic inhibition in the hippocampus supports fear learning. Science (New York, N.Y.) *343*, 857–863.
18. Turi, G.F., Li, W.K., Chavlis, S., Pandi, I., O'Hare, J., Priestley, J.B., Grosmark, A.D., Liao, Z., Ladow, M., Zhang, J.F., et al. (2019). Vasoactive Intestinal Polypeptide-Expressing Interneurons in the Hippocampus Support Goal-Oriented Spatial Learning. Neuron *101*, 1150–1165.e8.
19. Caroni, P. (2015). Inhibitory microcircuit modules in hippocampal learning. Curr. Opin. Neurobiol. *35*, 66–73.
20. Lasseter, H.C., Xie, X., Ramirez, D.R., and Fuchs, R.A. (2010). Sub-region specific contribution of the ventral hippocampus to drug context-induced reinstatement of cocaine-seeking behavior in rats. Neuroscience *171*, 830–839.
21. Xu, C., Krabbe, S., Gründemann, J., Botta, P., Fadok, J.P., Osakada, F., Saur, D., Grewe, B.F., Schnitzer, M.J., Callaway, E.M., and Lüthi, A. (2016). Distinct Hippocampal Pathways Mediate Dissociable Roles of Context in Memory Retrieval. Cell *167*, 961–972.e16.
22. Moser, M.B., and Moser, E.I. (1998). Functional differentiation in the hippocampus. Hippocampus *8*, 608–619.
23. Jung, M.W., Wiener, S.I., and McNaughton, B.L. (1994). Comparison of spatial firing characteristics of units in dorsal and ventral hippocampus of the rat. J. Neurosci. *14*, 7347–7356.
24. Kjelstrup, K.B., Solstad, T., Brun, V.H., Hafting, T., Leutgeb, S., Witter, M.P., Moser, E.I., and Moser, M.B. (2008). Finite scale of spatial representation in the hippocampus. Science (New York, N.Y.) *321*, 140–143.
25. Royer, S., Sirota, A., Patel, J., and Buzsáki, G. (2010). Distinct representations and theta dynamics in dorsal and ventral hippocampus. J. Neurosci. *30*, 1777–1787.
26. Komorowski, R.W., Garcia, C.G., Wilson, A., Hattori, S., Howard, M.W., and Eichenbaum, H. (2013). Ventral hippocampal neurons are shaped by experience to represent behaviorally relevant contexts. J. Neurosci. *33*, 8079–8087.
27. Ciocchi, S., Passecker, J., Malagon-Vina, H., Mikus, N., and Klausberger, T. (2015). Brain computation. Selective information routing by ventral hippocampal CA1 projection neurons. Science (New York, N.Y.) *348*, 560–563.
28. Spellman, T., Rigotti, M., Ahmari, S.E., Fusi, S., Gogos, J.A., and Gordon, J.A. (2015). Hippocampal-prefrontal input supports spatial encoding in working memory. Nature *522*, 309–314.
29. Place, R., Farovik, A., Brockmann, M., and Eichenbaum, H. (2016). Bidirectional prefrontal-hippocampal interactions support context-guided memory. Nat. Neurosci. *19*, 992–994.
30. Jimenez, J.C., Su, K., Goldberg, A.R., Luna, V.M., Biane, J.S., Ordek, G., Zhou, P., Ong, S.K., Wright, M.A., Zweifel, L., et al. (2018). Anxiety Cells in a Hippocampal-Hypothalamic Circuit. Neuron *97*, 670–683.e6.
31. Jimenez, J.C., Berry, J.E., Lim, S.C., Ong, S.K., Kheirbek, M.A., and Hen, R. (2020). Contextual fear memory retrieval by correlated ensembles of ventral CA1 neurons. Nat. Commun. *11*, 3492.
32. Forro, T., Volitaki, E., Malagon-Vina, H., Klausberger, T., Nevian, T., and Ciocchi, S. (2022). Anxiety-related activity of ventral hippocampal interneurons. Prog. Neurobiol. *219*, 102368.
33. Swanson, L.W., and Cowan, W.M. (1977). An autoradiographic study of the organization of the efferent connections of the hippocampal formation in the rat. J. Comp. Neurol. *172*, 49–84.
34. Gergues, M.M., Han, K.J., Choi, H.S., Brown, B., Clausing, K.J., Turner, V.S., Vainchtein, I.D., Molofsky, A.V., and Kheirbek, M.A. (2020). Circuit and molecular architecture of a

ventral hippocampal network. Nat. Neurosci. *23*, 1444–1452.
35. Shpokayte, M., McKissick, O., Guan, X., Yuan, B., Rahsepar, B., Fernandez, F.R., Ruesch, E., Grella, S.L., White, J.A., Liu, X.S., and Ramirez, S. (2022). Hippocampal cells segregate positive and negative engrams. Commun. Biol. *5*, 1009.
36. Britt, J.P., Benaliouad, F., McDevitt, R.A., Stuber, G.D., Wise, R.A., and Bonci, A. (2012). Synaptic and behavioral profile of multiple glutamatergic inputs to the nucleus accumbens. Neuron *76*, 790–803.
37. Okuyama, T., Kitamura, T., Roy, D.S., Itohara, S., and Tonegawa, S. (2016). Ventral CA1 neurons store social memory. Science (New York, N.Y.) *353*, 1536–1541.
38. LeGates, T.A., Kvarta, M.D., Tooley, J.R., Francis, T.C., Lobo, M.K., Creed, M.C., and Thompson, S.M. (2018). Reward behaviour is regulated by the strength of hippocampus-nucleus accumbens synapses. Nature *564*, 258–262.
39. Zhou, Y., Zhu, H., Liu, Z., Chen, X., Su, X., Ma, C., Tian, Z., Huang, B., Yan, E., Liu, X., and Ma, L. (2019). A ventral CA1 to nucleus accumbens core engram circuit mediates conditioned place preference for cocaine. Nat. Neurosci. *22*, 1986–1999.
40. Whissell, P.D., Cajanding, J.D., Fogel, N., and Kim, J.C. (2015). Comparative density of CCK- and PV-GABA cells within the cortex and hippocampus. Front. Neuroanat. *9*, 124.
41. Basu, J., Srinivas, K.V., Cheung, S.K., Taniguchi, H., Huang, Z.J., and Siegelbaum, S.A. (2013). A cortico-hippocampal learning rule shapes inhibitory microcircuit activity to enhance hippocampal information flow. Neuron *79*, 1208–1221.
42. Basu, J., Zaremba, J.D., Cheung, S.K., Hitti, F.L., Zemelman, B.V., Losonczy, A., and Siegelbaum, S.A. (2016). Gating of hippocampal activity, plasticity, and memory by entorhinal cortex long-range inhibition. Science (New York, N.Y.) *351*, aaa5694.
43. Loureiro, M., Renard, J., Zunder, J., and Laviolette, S.R. (2015). Hippocampal cannabinoid transmission modulates dopamine neuron activity: impact on rewarding memory formation and social interaction. Neuropsychopharmacology *40*, 1436–1447.
44. Del Pino, I., Brotons-Mas, J.R., Marques-Smith, A., Marighetto, A., Frick, A., Marín, O., and Rico, B. (2017). Abnormal wiring of CCK^{+} basket cells disrupts spatial information coding. Nat. Neurosci. *20*, 784–792.
45. Forro, T., and Klausberger, T. (2023). Differential behavior-related activity of distinct hippocampal interneuron types during odor-associated spatial navigation. Neuron *111*, 2399–2413.e5.
46. Taniguchi, H., He, M., Wu, P., Kim, S., Paik, R., Sugino, K., Kvitsiani, D., Fu, Y., Lu, J., Lin, Y., et al. (2011). A resource of Cre driver lines for genetic targeting of GABAergic neurons in cerebral cortex. Neuron *71*, 995–1013.
47. Murugan, M., Jang, H.J., Park, M., Miller, E.M., Cox, J., Taliaferro, J.P., Parker, N.F., Bhave, V., Hur, H., Liang, Y., et al. (2017). Combined Social and Spatial Coding in a Descending Projection from the Prefrontal Cortex. Cell *171*, 1663–1677.e16.
48. Donato, F., Rompani, S.B., and Caroni, P. (2013). Parvalbumin-expressing basket-cell network plasticity induced by experience regulates adult learning. Nature *504*, 272–276.
49. Stefanelli, T., Bertollini, C., Lüscher, C., Muller, D., and Mendez, P. (2016). Hippocampal Somatostatin Interneurons Control the Size of Neuronal Memory Ensembles. Neuron *89*, 1074–1085.
50. Hefft, S., and Jonas, P. (2005). Asynchronous GABA release generates long-lasting inhibition at a hippocampal interneuron-principal neuron synapse. Nat. Neurosci. *8*, 1319–1328.
51. Daw, M.I., Tricoire, L., Erdelyi, F., Szabo, G., and McBain, C.J. (2009). Asynchronous transmitter release from cholecystokinin-containing inhibitory interneurons is widespread and target-cell independent. J. Neurosci. *29*, 11112–11122.
52. Bartos, M., and Elgueta, C. (2012). Functional characteristics of parvalbumin- and cholecystokinin-expressing basket cells. J. Physiol. *590*, 669–681.
53. Dudok, B., Klein, P.M., Hwaun, E., Lee, B.R., Yao, Z., Fong, O., Bowler, J.C., Terada, S., Sparks, F.T., Szabo, G.G., et al. (2021). Alternating sources of perisomatic inhibition during behavior. Neuron *109*, 997–1012.e9.
54. Whissell, P.D., Bang, J.Y., Khan, I., Xie, Y.F., Parfitt, G.M., Grenon, M., Plummer, N.W., Jensen, P., Bonin, R.P., and Kim, J.C. (2019). Selective Activation of Cholecystokinin-Expressing GABA (CCK-GABA) Neurons Enhances Memory and Cognition. eNeuro *6*. ENEURO.0360-18.2019.
55. Wickersham, I.R., Finke, S., Conzelmann, K.K., and Callaway, E.M. (2007). Retrograde neuronal tracing with a deletion-mutant rabies virus. Nat. Methods *4*, 47–49.
56. Dimidschstein, J., Chen, Q., Tremblay, R., Rogers, S.L., Saldi, G.A., Guo, L., Xu, Q., Liu, R., Lu, C., Chu, J., et al. (2016). A viral strategy for targeting and manipulating interneurons across vertebrate species. Nat. Neurosci. *19*, 1743–1749.
57. Awatramani, R., Soriano, P., Rodriguez, C., Mai, J.J., and Dymecki, S.M. (2003). Cryptic boundaries in roof plate and choroid plexus identified by intersectional gene activation. Nat. Genet. *35*, 70–75.
58. Kim, J.C., Cook, M.N., Carey, M.R., Shen, C., Regehr, W.G., and Dymecki, S.M. (2009). Linking genetically defined neurons to behavior through a broadly applicable silencing allele. Neuron *63*, 305–315.
59. Nunzi, M.G., Gorio, A., Milan, F., Freund, T.F., Somogyi, P., and Smith, A.D. (1985). Cholecystokinin-immunoreactive cells form symmetrical synaptic contacts with pyramidal and nonpyramidal neurons in the hippocampus. J. Comp. Neurol. *237*, 485–505.
60. Cope, D.W., Maccaferri, G., Márton, L.F., Roberts, J.D.B., Cobden, P.M., and Somogyi, P. (2002). Cholecystokinin-immunopositive basket and Schaffer collateral-associated interneurones target different domains of pyramidal cells in the CA1 area of the rat hippocampus. Neuroscience *109*, 63–80.
61. Pawelzik, H., Hughes, D.I., and Thomson, A.M. (2002). Physiological and morphological diversity of immunocytochemically defined parvalbumin- and cholecystokinin-positive interneurones in CA1 of the adult rat hippocampus. J. Comp. Neurol. *443*, 346–367.
62. Tye, K.M., Mirzabekov, J.J., Warden, M.R., Ferenczi, E.A., Tsai, H.C., Finkelstein, J., Kim, S.Y., Adhikari, A., Thompson, K.R., Andalman, A.S., et al. (2013). Dopamine neurons modulate neural encoding and expression of depression-related behaviour. Nature *493*, 537–541.
63. Kubik, S., Miyashita, T., and Guzowski, J.F. (2007). Using immediate-early genes to map hippocampal subregional functions. Learn. Mem. *14*, 758–770.
64. Phillips, M.L., Robinson, H.A., and Pozzo-Miller, L. (2019). Ventral hippocampal projections to the medial prefrontal cortex regulate social memory. Elife *8*, e44182.
65. Moy, S.S., Nadler, J.J., Perez, A., Barbaro, R.P., Johns, J.M., Magnuson, T.R., Piven, J., and Crawley, J.N. (2004). Sociability and preference for social novelty in five inbred strains: an approach to assess autistic-like behavior in mice. Gene Brain Behav. *3*, 287–302.
66. Schultz, W. (2015). Neuronal Reward and Decision Signals: From Theories to Data. Physiol. Rev. *95*, 853–951.
67. Keiflin, R., and Janak, P.H. (2015). Dopamine Prediction Errors in Reward Learning and Addiction: From Theory to Neural Circuitry. Neuron *88*, 247–263.
68. Halahakoon, D.C., Kieslich, K., O'Driscoll, C., Nair, A., Lewis, G., and Roiser, J.P. (2020). Reward-Processing Behavior in Depressed Participants Relative to Healthy Volunteers: A Systematic Review and Meta-analysis. JAMA Psychiatr. *77*, 1286–1295.
69. Cembrowski, M.S., Wang, L., Sugino, K., Shields, B.C., and Spruston, N. (2016). Hipposeq: a comprehensive RNA-seq database of gene expression in hippocampal principal neurons. Elife *5*, e14997.
70. Bienkowski, M.S., Bowman, I., Song, M.Y., Gou, L., Ard, T., Cotter, K., Zhu, M., Benavidez, N.L., Yamashita, S., Abu-Jaber, J., et al. (2018). Integration of gene expression and brain-wide connectivity reveals the multiscale organization of mouse hippocampal networks. Nat. Neurosci. *21*, 1628–1643.
71. Robinson, T.E., and Berridge, K.C. (1993). The neural basis of drug craving: an incentive-sensitization theory of addiction. Brain Res. Brain Res. Rev. *18*, 247–291.
72. Ito, R., Robbins, T.W., Pennartz, C.M., and Everitt, B.J. (2008). Functional interaction between the hippocampus and nucleus accumbens shell is necessary for the acquisition of appetitive spatial context conditioning. J. Neurosci. *28*, 6950–6959.
73. Lansink, C.S., Goltstein, P.M., Lankelma, J.V., McNaughton, B.L., and Pennartz, C.M. (2009). Hippocampus leads ventral striatum in replay of place-reward information. PLoS Biol. *8*, e1000173.
74. van der Meer, M.A.A., and Redish, A.D. (2011). Theta phase precession in rat ventral striatum links place and reward information. J. Neurosci. *31*, 2843–2854.
75. Xia, L., Nygard, S.K., Sobczak, G.G., Hourguettes, N.J., and Bruchas, M.R. (2017). Dorsal-CA1 Hippocampal Neuronal Ensembles Encode Nicotine-Reward Contextual Associations. Cell Rep. *19*, 2143–2156.
76. Sjulson, L., Peyrache, A., Cumpelik, A., Cassataro, D., and Buzsáki, G. (2018). Cocaine Place Conditioning Strengthens Location-Specific Hippocampal Coupling to the Nucleus Accumbens. Neuron *98*, 926–934.e5.
77. Trouche, S., Koren, V., Doig, N.M., Ellender, T.J., El-Gaby, M., Lopes-Dos-Santos, V., Reeve, H.M., Perestenko, P.V., Garas, F.N., Magill, P.J., et al. (2019). A Hippocampus-Accumbens Tripartite Neuronal Motif Guides

Appetitive Memory in Space. Cell *176*, 1393–1406.e16.

78. Lavoie, A.M., and Mizumori, S.J. (1994). Spatial, movement- and reward-sensitive discharge by medial ventral striatum neurons of rats. Brain Res. *638*, 157–168.
79. Calipari, E.S., Bagot, R.C., Purushothaman, I., Davidson, T.J., Yorgason, J.T., Peña, C.J., Walker, D.M., Pirpinias, S.T., Guise, K.G., Ramakrishnan, C., et al. (2016). In vivo imaging identifies temporal signature of D1 and D2 medium spiny neurons in cocaine reward. Proc. Natl. Acad. Sci. USA *113*, 2726–2731.
80. Babl, S.S., Rummell, B.P., and Sigurdsson, T. (2019). The spatial extent of optogenetic silencing in transgenic mice expressing channelrhodopsin in inhibitory interneurons. Cell Rep. *29*, 1381–1395.e4.
81. Herman, A.M., Huang, L., Murphey, D.K., Garcia, I., and Arenkiel, B.R. (2014). Cell type-specific and time-dependent light exposure contribute to silencing in neurons expressing Channelrhodopsin-2. Elife *3*, e01481.
82. Kim, H., Ährlund-Richter, S., Wang, X., Deisseroth, K., and Carlén, M. (2016). Prefrontal parvalbumin neurons in control of attention. Cell *164*, 208–218.
83. Jun, N.Y., and Cardin, J.A. (2020). Activation of distinct channelrhodopsin variants engages different patterns of network activity. eNeuro *7*. ENEURO.0222-18.2019.
84. Baleisyte, A., Schneggenburger, R., and Kochubey, O. (2022). Stimulation of medial amygdala GABA neurons with kinetically different channelrhodopsins yields opposite behavioral outcomes. Cell Rep. *39*, 110850.
85. Varga, C., Lee, S.Y., and Soltesz, I. (2010). Target-selective GABAergic control of entorhinal cortex output. Nat. Neurosci. *13*, 822–824.
86. Klausberger, T. (2009). GABAergic interneurons targeting dendrites of pyramidal cells in the CA1 area of the hippocampus. Eur. J. Neurosci. *30*, 947–957.
87. Dudok, B., Barna, L., Ledri, M., Szabó, S.I., Szabadits, E., Pintér, B., Woodhams, S.G., Henstridge, C.M., Balla, G.Y., Nyilas, R., et al. (2015). Cell-specific STORM super-resolution imaging reveals nanoscale organization of cannabinoid signaling. Nat. Neurosci. *18*, 75–86.
88. Armstrong, C., and Soltesz, I. (2012). Basket cell dichotomy in microcircuit function. J. Physiol. *590*, 683–694.
89. Katona, I., Sperlágh, B., Sík, A., Käfalvi, A., Vizi, E.S., Mackie, K., and Freund, T.F. (1999). Presynaptically located CB1 cannabinoid receptors regulate GABA release from axon terminals of specific hippocampal interneurons. J. Neurosci. *19*, 4544–4558.
90. Marsicano, G., and Lutz, B. (1999). Expression of the cannabinoid receptor CB1 in distinct neuronal subpopulations in the adult mouse forebrain. Eur. J. Neurosci. *11*, 4213–4225.
91. Pitler, T.A., and Alger, B.E. (1994). Depolarization-induced suppression of GABAergic inhibition in rat hippocampal pyramidal cells: G protein involvement in a presynaptic mechanism. Neuron *13*, 1447–1455.
92. Jappy, D., Valiullina, F., Draguhn, A., and Rozov, A. (2016). GABABR-Dependent Long-Term Depression at Hippocampal Synapses between CB1-Positive Interneurons and CA1 Pyramidal Cells. Front. Cell. Neurosci. *10*, 4.
93. Wilson, R.I., and Nicoll, R.A. (2001). Endogenous cannabinoids mediate retrograde signalling at hippocampal synapses. Nature *410*, 588–592.
94. Losonczy, A., Biró, A.A., and Nusser, Z. (2004). Persistently active cannabinoid receptors mute a subpopulation of hippocampal interneurons. Proc. Natl. Acad. Sci. USA *101*, 1362–1367.
95. Carter, E., and Wang, X.J. (2007). Cannabinoid-mediated disinhibition and working memory: dynamical interplay of multiple feedback mechanisms in a continuous attractor model of prefrontal cortex. Cerebr. Cortex *17*, i16–i26.
96. Medrihan, L., Sagi, Y., Inde, Z., Krupa, O., Daniels, C., Peyrache, A., and Greengard, P. (2017). Initiation of Behavioral Response to Antidepressants by Cholecystokinin Neurons of the Dentate Gyrus. Neuron *95*, 564–576.e4.
97. James, T.A., Weiss-Cowie, S., Hopton, Z., Verhaeghen, P., Dotson, V.M., and Duarte, A. (2021). Depression and episodic memory across the adult lifespan: A meta-analytic review. Psychol. Bull. *147*, 1184–1214.
98. Torregrossa, M.M., Corlett, P.R., and Taylor, J.R. (2011). Aberrant learning and memory in addiction. Neurobiol. Learn. Mem. *96*, 609–623.
99. Herbener, E.S. (2008). Emotional memory in schizophrenia. Schizophr. Bull. *34*, 875–887.

STAR★METHODS

KEY RESOURCES TABLE

REAGENT or RESOURCE	SOURCE	IDENTIFIER
Antibodies		
Rabbit polyclonal anti-CCK	Sigma-Aldrich	Cat# C2581; RRID: AB_258806
Rabbit polyclonal anti-GABA	Sigma-Aldrich	Cat # A2052; RRID: AB_477652
Rabbit polyclonal anti-PV	Abcam	Cat# ab11427; RRID: AB_298032
Rabbit polyclonal anti-vasoactive intestinal peptide	Immunostar	Cat# 20077; RRID: AB_572270
Rat monoclonal anti-somatostatin	Millipore	Cat# MAB354; RRID: AB_2255365
Rabbit polyclonal anti-cFos	Santa Cruz Biotechnology	N/A
Chicken polyclonal anti-GFP	Abcam	Cat# ab13970; RRID: AB_300798
Goat polyclonal anti-mCherry	Sicgen	Cat# AB0040-200; RRID: AB_2333093
AlexaFluor-488-conjugated donkey anti-rabbit	Jackson ImmunoResearch Laboratories	Cat# 711545152; RRID: AB_2313584
AlexaFluor-594-conjugated donkey anti-rabbit	Jackson ImmunoResearch Laboratories	Cat# 711585152; RRID: AB_2340621
Cy5-conjugated donkey anti-rabbit	Jackson ImmunoResearch Laboratories	Cat# 711175152; RRID: AB_2340607
DyLight-405-conjugated donkey anti-rabbit	Jackson ImmunoResearch Laboratories	Cat# 711475152; RRID: AB_2340616
AlexaFluor-488-conjugated donkey anti-chicken	Jackson ImmunoResearch Laboratories	Cat# 703545155; RRID: AB_2340375
AlexaFluor-594-conjugated donkey anti-goat	Jackson ImmunoResearch Laboratories	Cat# 705585003; RRID: AB_2340432
Bacterial and virus strains		
AAV2/5-CaMKIIα-eArchT3.0-EYFP	UNC Vector Core	N/A
AAV2/5-CAMKIIα-EYFP	UNC Vector Core	N/A
CAV2-cre	Plateforme de Vectorologie de Montpellier	N/A
AAV2/8-EF1α-DIO-TC66T-2A-EGFP-2A-oG	GT3 Viral Core Facility of the Salk Institute	N/A
EnvA-RVdG-mCherry	GT3 Viral Core Facility of the Salk Institute	N/A
AAV2/1-Dlx5/6-DIO-ChR2-EGFP	Vigene Biosciences	N/A
Chemicals, peptides, and recombinant proteins		
Cholera toxin subunit B conjugated to Alexfluor-555	Invitrogen	C34776
Red retrobeads	Lumafluor Inc.	N/A
Experimental models: Organisms/strains		
CCK-ires-Cre (*Cck*$^{tm1.1(cre)Zjh}$/J)	The Jackson Laboratory	012706
Dlx5/6-Flpe (Tg(mI56i-flpe)39Fsh/J)	The Jackson Laboratory	010815
C57BL/6-Tg(Gt(ROSA)26Sor-ArchT/EGFP)	Donated by Dr. Itaru Imayoshi	https://knowledge.brc.riken.jp/resource/animal/card?__lang__=en&brc_no=RBRC06585
Software and algorithms		
ImageJ2 Fiji 2.3.0	NIH	https://fiji.sc/
GraphPad Prism 9.5.1	Dotmatics	https://www.graphpad.com/
ANY-maze	Stoelting Co.	https://www.any-maze.com/
FreezeFrame 4	ActiMetrics	https://actimetrics.com/products/freezeframe/
Clampfit 10.7	Molecular Devices, LLC	https://www.moleculardevices.com/products/axon-patch-clamp-system/acquisition-and-analysis-software/pclamp-software-suite

RESOURCE AVAILABILITY

Lead contact

Further information and requests for resources and reagents should be directed to and will be fulfilled by the lead contact, Jun Chul Kim (junchul.kim@utoronto.ca).

Materials availability

This study did not generate new unique reagents.

Data and code availability

- All data reported in this paper will be shared by the lead contact upon request.
- This paper does not report original code.
- Any additional information required to reanalyze the data reported in this paper is available from the lead contact upon request.

EXPERIMENTAL MODEL AND STUDY PARTICIPANT DETAILS

Triple transgenic *CCK-Cre;Dlx5/6-Flpe;RC::PFArchT-EGFP* mice (termed CCK-ArchT mice) were generated as follows: *Dlx5/6-FLPe* mice were crossed with homozygous CCK-ires-Cre mice to generate double transgenic *Dlx5/6-Flpe;CCK-Cre* mice, which were then crossed with *RC::PFArchT-EGFP* mice (obtained from the laboratory of Dr. Itaru Imayoshi). C57BL/6J mice (Charles River Laboratories) were used as subjects for optogenetic pathway targeting, rabies tracing, and cFos experiments. Mice were group-housed in a temperature- and humidity-controlled environment, and a 12-hour light/dark cycle. They had *ad libitum* access to food and water unless otherwise specified. Surgery was performed on 4-month-old male mice, and behavioural tests were conducted up to the age of 6 months. All experimental procedures were conducted in accordance with the guidelines of the Canadian Council on Animal Care (CCAC) and approved by the Local Animal Care Committees of the University of Toronto (Toronto, Ontario, Canada).

METHOD DETAILS

Stereotaxic surgery

Mice were anaesthetized with isoflurane and mounted onto a stereotaxic frame. For optogenetic inhibition of ventral CA1 terminals in the nucleus accumbens, AAV2/5-CaMKIIα-eArchT3.0-EYFP or AAV2/5-CAMKIIα-EYFP (0.3 μL, UNC Vector Core) was bilaterally infused into the ventral hippocampus (AP: -2.90 mm, DV: -4.90, ML: ± 3.30 mm), and optic fibres were implanted bilaterally above the nucleus accumbens shell AP: 1.60 mm, DV: -4.00, ML: ±0.60 mm). For transsynaptic rabies tracing experiments, wildtype C57BL6/J mice were unilaterally infused with CAV2-cre (0.5 μL, Plateforme de Vectorologie de Montpellier) into the NAc (AP: 1.60 mm, DV: -4.75, ML: ±0.60 mm), and with AAV2/8-EF1α-DIO-TC66T-2A-EGFP-2A-oG (0.3 μL, GT3 Viral Core Facility of the Salk Institute) into the left or right ventral CA1/subiculum. Two weeks later, EnvA-RVdG-mCherry (0.7 μL, GT3 Viral Core Facility of the Salk Institute) was infused into the same hemisphere of the ventral CA1/subiculum. For *ex vivo* electrophysiology experiments, CCK-Cre mice were bilaterally infused with AAV2/1-Dlx5/6-DIO-ChR2-EGFP (0.3 μL, Vigene Biosciences, custom production) into the ventral CA1/subiculum and with rhodamine retrobeads (590 nm, 1 μL, Lumafluor Inc.) into the nucleus accumbens. For optogenetic experiments with CCK-Cre/DLX5/6-Flp/PFArchT mice, optic fibres were implanted bilaterally above the ventral CA1/subiculum region (AP: -2.90 mm, DV: -4.10, ML: ± 3.30 mm). For retrograde tracing experiments in combination with cFos labeling, cholera toxin subunit B conjugated to Alexfluor-555 (CTB-555, 0.7 μL, Invitrogen) was infused unilaterally into the NAc of CCK-ArchT mice. Infusions were made via an internal cannula (31 gauge) in the target region connected by tubing to a 10 uL Hamilton syringe. The internal cannula was left in place for 10 minutes after infusion to prevent solution backflow. Optic fibres were secured to the skull using dental cement (RelyX Unicem; 3M). After surgery, mice were individually housed and allowed a minimum of 1 week to recover before behavioural experiments. The brain coordinates described are in reference to Paxinos and Franklin (2007).

Behavioural Apparatuses and testing procedures

Experimental Timeline

For optogenetic inhibition of vHPC-NAc terminals, C57BL/6J littermate mice were randomly assigned to the EYFP (N = 8) and ArchT (N = 9) group and solely underwent sucrose conditioned place preference (procedures described subsequently). For the cFos experiment without optogenetic manipulation, C57BL/6J littermate mice were randomly assigned to each of the following conditions: home-cage (N = 5), Reward-Alone (N = 5), Neutral Context (N = 5), Context + Reward (N = 5). For the cFos experiment with CCK interneuron inhibition, littermate CCK-ArchT- (N = 6) and CCK-ArchT+ (N = 5) were injected with CTB-555 in the NAc and implanted with an optic fibre in the ipsilateral vCA1. One CCK-ArchT- subject was excluded from CTB-555/cFos cell quantification due to mistargeting of the CTB-555 injection. For CCK interneuron inhibition with behavioural testing, 2 experimental cohorts of CCK-ArchT- and CCK-ArchT+ littermates were prepared. The first cohort of CCK-ArchT- (N = 8) and CCK-ArchT+ (N = 9) underwent sucrose conditioned place preference, followed 1 month later by contextual fear conditioning which was conducted in a separate testing room and apparatus. The second cohort of CCK-ArchT- (N = 8) and CCK-ArchT+ (N = 5) mice underwent repeated real-time place preference. One month later, intact healthy mice were tested for social recognition memory (CCK-ArchT-, N = 6) and CCK-ArchT+, N = 4).

General procedures

One week after recovery from stereotaxic surgery, mice who underwent optogenetic behavioural testing were individually handled for 5 minutes on 3 consecutive days. On the last day of handling, mice were acclimated to being tethered to the optical patch cords for 5 minutes in the behavioural testing room. Behavioural tests were conducted during the light phase of the cycle, under room lighting (100 lux), and tracked and scored using ANY-maze™ (Stoelting Co.) or FreezeFrame 4 (Coulbourne Instruments) for freezing behaviour. Apparatuses were cleaned with 70% ethanol before the introduction of each individual mouse unless otherwise specified. For optogenetic inhibition, 532 nm of laser light was set to a power of 15 mW from the fibre tip and delivered continuously, either throughout the apparatus or in a particular compartment as described in the specific behavioural methods below.

Sucrose conditioned place preference

To test for changes in learning of context-reward associations, sucrose conditioned place preference was performed. Conditioned place preference for sucrose solution (1% or 10% in water) was tested in a rectangular chamber comprised of two contexts (each 25 cm L x 20 cm W x 30 cm H) with mice having free access to both contexts. The walls of each context had a pattern that was either black and white horizontal stripes or black spots, and the floor was one of two metal textures. One day prior to training, mice were tested for their baseline preference of the two contexts in a 5-minute session (Pre-Train Test). During training, the less preferred context contained sucrose solution and the preferred side contained water. A petri dish (6 cm diameter) was filled with each solution (10 ml) and placed into either context at the far opposing walls. Mice were placed into the light-unpaired side facing the wall and allowed to explore for 15 minutes. Light was delivered upon entry into the sucrose-paired context as measured from the body's centre point. Solutions were weighed before and after training to measure the amount of consumption during training. Mice were trained over 3 consecutive sessions. Forty-eight hours after the last session, a 5 minute preference test was conducted (Post-Train Test). For this test, mice were first food and water deprived for 16 hours.

Contextual fear conditioning

The contextual fear task was conducted in arenas placed inside of sound-attenuating boxes (Med Associates Inc.). Two unique arenas (contexts) were used which differed in their visual, tactile, and olfactory cues. The fear conditioning context (context A) was a square arena (30 cm L x 24 cm W x 21 cm H) that had walls constructed of metal and clear plastic, a metal grid floor (19 stainless steel rods), and a house light, and was cleaned with 70% ethanol. The neutral context (context B) was semicircular in shape and was made of smooth white plastic (30 cm wide) and was cleaned with 4% acetic acid. During conditioning on day 1, mice were placed into context A for a total of 300 seconds during which 2 footshocks (2 s, 0.7 mA) were delivered at timepoints 180 and 240 seconds into the session. The next day, mice were returned to context A for 300 seconds during which freezing was measured as an index of contextual fear memory. On day 3, mice were placed into the novel context B for 300 seconds during which freezing was measured as index of contextual fear memory generalization. Freezing (minimum bout duration of 0.5 s) was automatically scored using tracking software (FreezeFrame 4, ActiMetrics).

Social recognition memory

Social memory was tested in a three-chamber social recognition memory test.[65] The apparatus was made of clear Plexiglas and consisted of three chambers, each measuring 40 cm L × 20 cm W × 40 cm H. The two side chambers contained a cylindrical wire cage (10.5 cm D × 11 cm H, 1 cm bar spacing). Subjects were able to freely move between chambers through an opening (5 cm × 40 cm) in the partitioning walls. Subject mice were placed into the centre chamber and allowed to acclimate to the entire apparatus for 10 minutes. Following acclimation, a 4-week old adolescent male C57BL/6 mouse, unfamiliar to the subject, was placed into a cage in one of the side chambers and interaction was permitted for 5 minutes. Immediately following this phase, the subject was confined to the centre while a second unfamiliar mouse was placed in the previously empty cage. Interaction was again permitted for 5 minutes to test for social recognition memory. Interaction was manually scored by key presses as any directed nose contact with the target mouse or cage. The initial unfamiliar mouse and chamber side were counterbalanced within control and CCK-ArchT groups.

cFos behavioural procedures

To examine vHPC neural activation associated with context-reward learning, we measured cFos expression after mice were exposed to specific events. In the first experiment, mice were either exposed to sucrose solution (1%, Reward-Alone) in their home-cage, to a familiarized context containing water (Neutral Context), or to the same context containing sucrose solution (1%, Context + Reward), or were gently and briefly handled in the home-cage (Home-Cage). Prior to the day of exposure, mice underwent 4 consecutive habituation days during which they were individually handled for 5 minutes and acclimated to the testing room in their home-cages for 2 hours. During the fourth day, mice in the Neutral Context and Context + Reward conditions were habituated to the experimental arena context (25 cm L x 20 cm W x 30 cm H) without water or sucrose for 5 minutes. On the fifth day, mice were first acclimated to the testing room for 2 hours in their home-cages and were then exposed to their respective conditions for 10 minutes. They were then returned to their home-cages for 60 minutes, after which they were immediately sacrificed. In the second experiment, to determine whether CCK interneuron inhibition during context-reward association learning affects vHPC neural activity, we analyzed cFos expression following exposure to a rewarding context with optogenetic inhibition of CCK interneurons. On the fourth day of handling and room habituation, mice were also connected to the optical patch cords and allowed to acclimate for 5 minutes in the home-cage. While tethered, they were habituated to the arena without reward

for 5 minutes, were untethered and returned to the home-cage in the testing room for another 2-hour period. On the fifth day, mice were habituated to the testing room for 2 hours and were then placed into the context with 1% sucrose solution and light delivery for 10 minutes. After testing, mice were returned to their home-cage and sacrificed 60 minutes later.

Ex vivo electrophysiology

Slice preparation

Mice were sacrificed at postnatal day 90-120 and 1-2 weeks after the final stereotaxic surgery in order to prepare acute brain slices for opto-physiological recording. We injected chloral hydrate solution (400 mg/kg) interperitoneally before decapitation. The brain was extracted into ice-cold oxygenated ACSF-sucrose solution (254 mM sucrose, 10 mM D-glucose, 24 mM $NaHCO_3$, 2 mM $CaCl_2$, 2 mM $MgSO_4$, 3 mM KCl, and 1.25 mM NaH_2PO_4, pH 7.4). A Dosaka Linear slicer was used to prepare ventrohippocampal coronal slices (~400 μm thick, Bregma -2.9mm to -3.8mm); each slice was transferred to a chilled ACSF-sucrose solution filled petri dish and halved at the midline. Slices were then transferred to an oxygenated recovery chamber filled with 30°C ACSF solution (128 mM NaCl, 10 mM D-glucose, 26 mM $NaHCO_3$, 2 mM $CaCl_2$, 2 mM $MgSO_4$, 3 mM KCl, and 1.25 mM NaH_2PO_4, pH 7.4). After >1 hour of post-slicing recovery, slices were placed on to a slice chamber and perfused with 30°C ACSF for optophysiological recordings.

Electrophysiological recordings

EGFP-positive CCK interneurons and retrobead-positive CA1 pyramidal cells in ventrohippocampal brain slices were identified respectively using a white-light collimated LED and FITC and TRITC filter cubes. Labelled neurons were targeted for patching using IR-DIC via 60x lens on a BX51WI microscope (Olympus). Pipettes (~2-4 MΩ) contained potassium gluconate (120 mM K-gluconate, 5 mM KCl, 2 mM $MgCl_2$, 4 mM K_2-ATP, 0.4 mM Na_2-GTP, 10 mM Na_2-phosphocreatine, and 10 mM HEPES buffer; pH 7.3). Whole cell patch clamp recordings were conducted using a HEKA EPC10 amplifier and Patchmaster software and were analyzed using Clampfit-10.7 (Molecular Devices, LLC). Channelrhodopsin was stimulated with light via a 445/45 nm excitation filter, delivered in 1 ms pulses to stimulate the somata of ChR2-EGFP+ CCK interneurons or 5 ms pulses to excite their axons terminating on retrobead$^{vHPC \rightarrow NAc}$ vCA1 pyramidal neurons.

Pharmacology

Drug manipulations to the slice during optophysiological experiments were administered via ACSF perfusion. Antagonists included the GABA-A blocker bicuculline methiodide (BCC, 3 μM, Tocris) by itself or, in a subset of neurons, BCC in combination with the GABA-B blocker CGP 35348 (CGP, 1 μM; Tocris). Antagonist was pre-applied for 5 minutes before and co-applied during the relevant optophysiological recording. To examine the recovery of the optophysiological effect upon partial washout, additional recordings were performed in a subset of neurons ~5-10 mins after BCC application ended.

Histology

Mice were transcardially perfused with PBS, pH 7.4, followed by 4% PFA. Brains were extracted and postfixed overnight in 4% PFA at 4°C and then cryoprotected with PBS containing 30% sucrose. Brains were sectioned coronally at 40 μm thickness using a cryostat (Leica Microsystems, CM 1520). For immunostaining, free-floating brain sections were blocked with 5% normal donkey serum in 0.1% Triton X-100 in PBS (PBS-T) for 2 h. Sections were then incubated for 48–72 h at 4°C with PBS-T containing a combination of the following primary antibodies: rabbit polyclonal anti-CCK-8 (1:1000, Sigma Millipore, C2581, rabbit anti-proCCK (Frontier Institute, Af350), rabbit polyclonal anti-GABA (1:1000, Sigma Millipore, A2052), rabbit polyclonal anti-PV antibody (1:1000, Abcam, ab11427), rabbit polyclonal anti-vasoactive intestinal peptide (VIP) (1:500, Immunostar, 20077), rat polyclonal anti-somatostatin (1:500, Millipore, MAB354), rabbit polyclonal anti-cFos (1:1000, Santa Cruz Biotechnology), chicken polyclonal anti-GFP (1:1000, Abcam, ab13970), and goat polyclonal anti-mCherry (1:1000, Sicgen, AB0040-200). Primary antibody incubation was followed by incubation for 2 h at room temperature with PBS-T containing the following secondary antibodies: AlexaFluor-488-conjugated donkey anti-rabbit (1:1000, Jackson ImmunoResearch Laboratories, 711545152), AlexaFluor-594-conjugated donkey anti-rabbit (1:1000, Jackson ImmunoResearch Laboratories, 715515152), Cy5-conjugated donkey anti-rabbit (1:1000, Jackson ImmunoResearch Laboratories, 711175152), DyLight-405-conjugated donkey anti-rabbit (1:500, Jackson ImmunoResearch Laboratories, 711475152), AlexaFluor-488-conjugated donkey anti-chicken (1:1000, Jackson ImmunoResearch Laboratories, 703545145), and AlexaFluor-594-conjugated donkey anti-goat (1:1000, Jackson ImmunoResearch Laboratories, 705515147). For cell counting experiments, every fourth section of the vHPC was collected and immunostained. The sections were mounted and imaged on a confocal laser scanning microscope with a 20× objective (Leica LSM 800). Fluorescent cells were counted in the ventral CA1 and subiculum (bregma -3.30 mm to -3.8 mm) in a 300 × 700 μM area using ImageJ2 Fiji.

QUANTIFICATION AND STATISTICAL ANALYSIS

Data were analyzed using One-way ANOVA, repeated measures ANOVA, Mixed ANOVA, and paired and unpaired Student's t-tests. Where appropriate, ANOVAs were followed by post-hoc tests. Statistical analyses were performed using GraphPad Prism 9.5.1. Statistical details of experiments can be found in the figure legends.